ISSN: 2710-0588

Flank Face Temperature Modeling of Chamfered Tool With the Influence of Dead Metal Zone

Honglin Leng, Binglin Li*

School of Mechatronic Engineering, Southwest Petroleum University, Chengdu, 610500, China

* Corresponding Author

Abstract

During the cutting process of chamfered tools, The Dead Metal Zone (DMZ) forms at the front of the chamfer, interacting with the workpiece through friction and generating an additional heat source that affects the tool's cutting temperature. This paper analyzes the cutting model of chamfered tools considering the effect of DMZ and establishes the relationship between cutting force and tool geometric parameters. The cutting force is used to determine the magnitude of the heat source during the cutting. Using the semi-boundary heat transfer principles, the temperature rise of the tool's flank face is calculated. Finite element simulations of chamfered tool cutting on AISI-1045 steel are conducted, and the resulting temperature rise is compared with theoretical calculations. The temperature distribution of the chamfered tool is obtained, along with the determination of heat source distribution coefficients and heat partition fractions on the flank face.

Keywords

Chamfered tool; Thermal modeling; Flank face temperature.

1. Introduction

The cutting theory model plays an important role in studying of relationship between cutting force and tool geometry parameters Merchant et al. [1] proposed the shear plane model, demonstrating the relationship between the friction angle, rake angle, and shear angle. Oxley et al. [2] proved that shear deformation occurs within a shear band of a certain width and established an orthogonal cutting model suitable for various cutting speeds. Fang et al. [3-4] proposed a cutting model considering the influence of tool-chip contact on the rake face and a model of corresponding negative rake angle. Karpat et al. [5] extended the modeling of the slip-line field in the negative rake angle chamfered tool. Hu et al. [6] treated DMZ as the tool's cutting edge and analyzed the cutting force model of chamfered tools. Zhuang et al. [7] proposed a double chamfered orthogonal cutting model and calculated the cutting force on both chamfers based on slip-line field theory. The various theoretical supports laid the foundation for in-depth research on cutting theory.

Improving the strength of the tool, Hitomi [8] proposed a cutting edge with a chamfered treatment. Jacobson et al. [9] found through experiments that during the machining process, the material flow speed at the tool chamfered edge is approximately zero, causing material to accumulate at the chamfered edge, referred to as the Dead Metal Zone (DMZ). The formation of the DMZ affects the cutting force, tool life, and cutting temperature distribution. Wan et al. [10], using slip-line field theory, determined the relationship between the edge length and vertex angle of the DMZ and the cutting edge geometry parameters. Wu et al. [11] pointed out the formation mechanism of the DMZ in chamfered tools, as well as the trends that cutting force increases with the chamfer angle and decreases with cutting speed.

ISSN: 2710-0588

During the cutting process, the cutting temperature directly affects tool life and surface quality of the workpiece. Komanduri et al. [12-14] developed analytical models of the cutting process and analyzed the influence of three heat sources—chip, workpiece, and tool—on tool temperature rise. Karpat et al. [15], by establishing a slip-line field, treated DMZ as a heat source and, by superimposing it with the three heat sources proposed by Komanduri, calculated the tool temperature rise during the cutting process. Yin et al. [16], based on experiments using chamfered PCBN tools for machining gray cast iron, demonstrated that cutting force and cutting temperature increase with higher cutting speed, cutting depth, and feed rate. Hussain et al. [17], through studies on the effect of chamfer size and geometric parameters on cutting temperature, observed that cutting temperature increases with the chamfer angle and chamfer width.

In this study, the temperature distribution and flank face temperature variation trend of chamfered tools during the cutting process of AISI-1045, an orthogonal cutting model of chamfered tools is used to establish the relationship between tool geometry parameters, cutting force, and heat source. Based on the heat source method by Komanduri and Hous, the heat source image formed by the friction between DMZ and the chamfered cutting edge, as well as the superimposition effect of the tool-chip friction heat source on the rake face, is analyzed to evaluate the impact on the temperature rise of chamfered tools. The finite element simulation results are used to determine the temperature distribution on the tool's flank face and the values of heat source distribution coefficients, thereby verifying the accuracy of the theoretical model.

2. Construction of the Orthogonal Cutting Model for Chamfered Tools

During the cutting process, the DMZ can be considered a new cutting edge that replaces the actual tool edge during cutting. Based on the slip-line field theory derived by Hu, the force conditions of the chamfered tool can be obtained, as shown in Fig.1 [6].

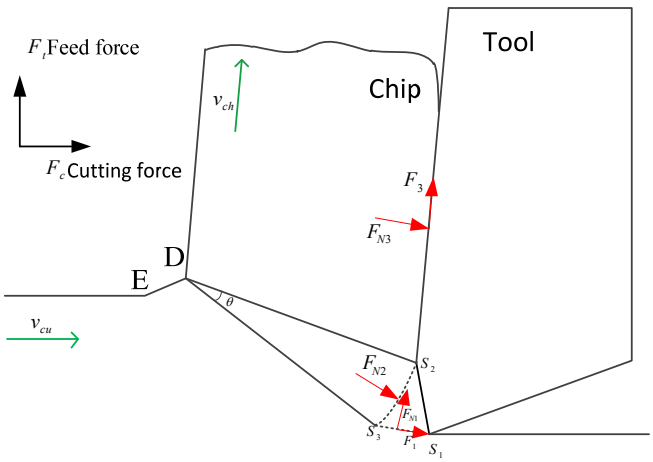

Figure 1. Force Diagram of the Chamfered Tool

From Fig.1, it can be observed that the triangular region $S_1S_2S_3$, bounded by arc S_1S_3, represents the DMZ formed during the cutting process of the chamfered tool. This region can be considered a stable rigid body. S_3 is identified as the apex of the DMZ, where material flow diverges: above S_3, chips are formed with a flow velocity of v_{ch}, while below S_3, the machined surface is generated, where the material flow velocity equals the cutting speed v_{cu}.

The forces acting within this region include:

1. F_{N1} and F_1, which are the normal and tangential forces at the DMZ boundary interacting with the material.

ISSN: 2710-0588

2. F_{N2}, the normal force generated chip-DMZ boundary.
3. F_3 and F_{N3}, which are the normal and tangential forces at the interface chip and rake face.
Its velocity vector hodograph is shown in Fig.2.

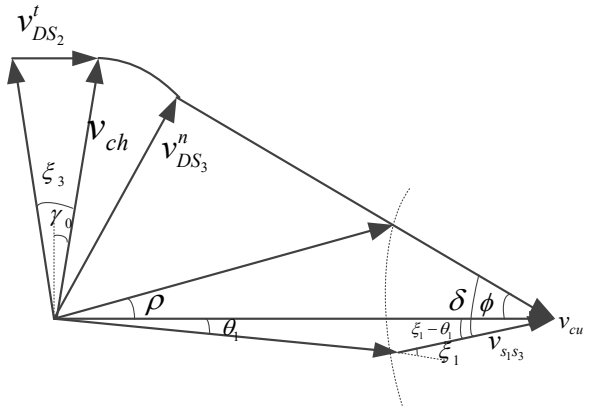

Figure 2. Velocity Vector Hodograph

Where γ_0 is the rake angle, ρ is the prow angle, represents the rising angle h when the material undergoes plastic deformation and transforms into a chip. θ_1 is the angle between the DMZ and the cutting velocity. The relationship among these three parameters is given by Eq.(1).

$$\sin\rho = \frac{\sin\theta_1}{\sqrt{2}\sin\xi_1} \tag{1}$$

ζ_1, ζ_2, andζ_3 are friction factor angles between the DMZ and rake face, DMZ and workpiece, as well as the chamfer. The friction factor angle calculation formulas for certain materials are shown in Table 1 [18]. θ represents the angle at which the material undergoes elastic-plastic deformation above point S_3, while φ is the shear angle.

Table1. Friction factor angle calculation formulas for some materials

materials	friction factor angleζ (deg)
AISI-1045	26.8-0.031v_{cu}+11.77h
Al7050-T7050	25.877-1283h-0.007v_{cu} +0.181γ_0
Al6061-T651-T651	20.835-4.901h-0.007v_{cu}+0.291γ_0

τ_1, τ_2, and τ_3 represent the shear stresses in the cutting model:
τ_1 is the shear stress at the lower boundary of DMZ and workpiece,
τ_2 is the shear stress at the front boundary of DMZ and chip,
τ_3 is the shear stress between the tool-chip.
The relationship is as follows:

$$\begin{cases} \tau_1 = k\cos(2\xi_1) \\ \tau_2 = k\cos(2\xi_2) \\ \tau_3 = k\cos(2\xi_3) \end{cases} \tag{2}$$

ISSN: 2710-0588

Where, k is the shear flow stress of the workpiece.

The relationship between the component forces and shear stress in the orthogonal cutting model is as follows:

$$\begin{cases} F_1 = kw\cos(2\xi_1)l_1 \\ F_{N1} = kw\left(1+2\theta+2(\varphi+\xi_1-\theta_1)+\sin(2\xi_1)\right)l_1 \\ F_{N2} = kw\left(1+2\theta+\sin(2\xi_3)\right)l_2 \\ F_3 = kw\cos(2\xi_3)l_4 \\ F_{N3} = kw\left(1+\sin(2\xi_3)\right)l_4 \end{cases} \tag{3}$$

Where w is the width of cutting, l_1 represents the length of DMZ boundary S_1S_3, l_2 represents the arc length of DMZ, l_3 represents the length of the primary shear plane in the slip-line field, and l_4 represents the contact length tool-chip [6]. These values are calculated using the following eq (4).

$$\begin{cases} l_1 = l_0 \dfrac{\sin\left(\psi+\dfrac{\theta}{2}\right)}{\sin\left(\varphi-\dfrac{\theta}{2}+\gamma_{01}\right)} \\ l_2 = \dfrac{h}{\sin\varphi} \\ l_3 = l_0 \dfrac{\sin\left(\varphi-\dfrac{\theta}{2}+\gamma_{01}\right)}{\sin\left(\psi+\dfrac{\theta}{2}\right)} \\ l_4 = \theta l_3 \end{cases} \tag{4}$$

Where γ_{01} is the chamfer angle. Based on geometric relationships, the feed force and cutting force acting on the tool can be expressed as follows:

$$\begin{cases} F_c = \cos(\theta_1)F_1 + \sin(\theta_1)F_{N1} + \\ \qquad \cos\left(\varphi-\dfrac{\theta}{2}\right)F_{N2} - \sin(\gamma_0)F_3 + \\ \qquad \cos(\gamma_0)F_{N3} \\ F_t = -\sin(\theta_1)F_1 + \cos(\theta_1)F_{N1} - \\ \qquad \sin\left(\varphi-\dfrac{\theta}{2}\right)F_{N2} + \cos(\gamma_0)F_3 + \\ \qquad \sin(\gamma_0)F_{N3} \end{cases} \tag{5}$$

Based on Eqs (3), (4), and (5), the material flow shear stress can be expressed in terms of two cutting stresses: shear stress k_1 and normal stress k_2.

ISSN: 2710-0588

$$k_1 = \frac{F_c}{w}\begin{bmatrix} F_3 \\ F_{N3} \\ F_{N2} \\ F_{N1} \\ F_1 \end{bmatrix}^T \begin{bmatrix} \sin(\gamma_0) \\ \cos(\gamma_0) \\ \cos\left(\varphi - \frac{\theta}{2}\right) \\ \sin(\theta_1) \\ \cos(\theta_1) \end{bmatrix}^{-1} \tag{6}$$

$$k_2 = \frac{F_t}{w}\begin{bmatrix} F_3 \\ F_{N3} \\ F_{N2} \\ F_{N1} \\ F_1 \end{bmatrix}^T \begin{bmatrix} \cos(\gamma_0) \\ \sin(\gamma_0) \\ -\sin\left(\varphi - \frac{\theta}{2}\right) \\ \cos(\theta_1) \\ \sin(\theta_1) \end{bmatrix}^{-1} \tag{7}$$

The total cutting stress k is expressed as:

$$k = \sqrt{(k_1^2 + k_2^2)} \tag{8}$$

3. Thermal Modeling Analysis in the Orthogonal Cutting Process of Chamfered Tools

3.1. Heat Source Analysis

During the cutting process, DMZ generates heat due to friction with the workpiece [6]. Therefore, the cutting heat in the chamfered tool The cutting process consists of three main heat sources: Q_{PHS}, the heat source from shear deformation in the primary deformation zone; Q_{THS}, the heat source from tool-chip contact; and Q_{SHS}, the heat source from the DMZ.,, as shown in Fig.3.

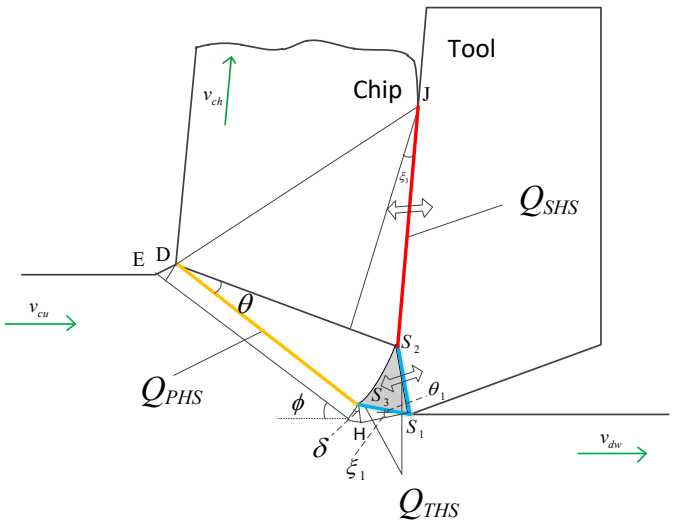

Figure 3. Schematic Diagram of chip and tool Heat Source Distribution

ISSN: 2710-0588

In the dry cutting process, the generated heat is primarily carried away by the chip, transferred into the tool, and absorbed by the workpiece. The temperature rise of the tool is mainly influenced by the two heat sources: Q_{SHS} (tool-chip contact heat source) and Q_{THS} (DMZ heat source).

(1) The temperature rise caused by Q_{SHS} (tool-chip contact region S_2J).

During the cutting process, the tool-chip contact heat source (Q_{SHS}) is considered a rectangular heat source, as shown in Figure 4. To account for the boundary effects of the chip when calculating the temperature rise, a image heat sources is introduced. The distribution of Q_{SHS} is illustrated in the fig4.

For a strip heat source Q_{SHS} with a width of *dzi* and a length of *dyi*, the temperature rise at point P (*x,y,z*) on the tool satisfies the following eqs(9),(10):

$$Q_{SHS} = \tau_2 V_{ch} = k\cos(2\xi_3)\frac{V_{cu}\sin(\phi)}{\cos(\xi_3)} \tag{9}$$

$$d\theta_t = \frac{B_1^c Q_{SHS}}{2\pi\lambda} dy_i \left(\frac{1}{R_i} + \frac{n}{R_i'}\right) dz_i \tag{10}$$

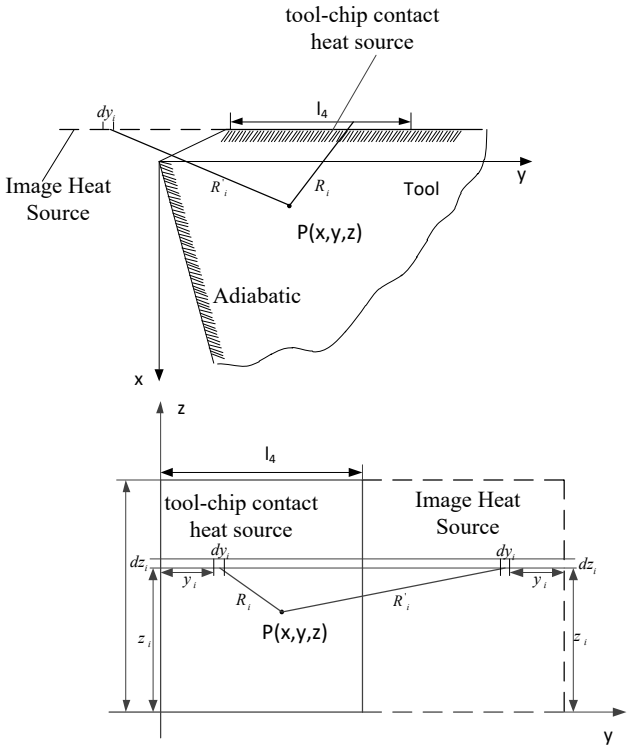

Figure 4. Effect of Tool-Chip Friction Heat Source on the Tool Temperature Field

In the dry cutting process, the tool can be considered adiabatic, so n=1. R_i and R'_i represent the distances from the heat source and its image heat sources to P (*x, y, z*), respectively. Their eqs are as follows:

$$R_i = \sqrt{x^2 + (y - x_i)^2 + (y - y_i)^2} \tag{11}$$

ISSN: 2710-0588

$$R_i^{'} = \sqrt{x^2 + \left(y - 2l_4 + y_i\right)^2 + \left(z - z_i\right)^2} \tag{12}$$

For a uniformly distributed strip heat source Q_{SHS} with a width of w and a length of l_4, the temperature rise at any point P (x, y, z) on the tool satisfies the following eq:

$$\theta_t = \frac{B_1^c Q_{SHS}}{2\pi\lambda} \int_0^{l_4} dy_i \int_0^w \left(\frac{1}{R_i} + \frac{1}{R_i^{'}} \right) dz_i \tag{13}$$

(2) The temperature rise caused by Q_{THS} (DMZ and chamfered boundary S_1S_2)

For a heat source Q_{THS} caused by the friction between DMZ and chamfered boundary S_1S_2, with a width of dxi and a length of dli, the temperature rise can be calculated accordingly.

$$Q_{THS} = \tau_1 V_{dw} = k \cos\left(2\xi_1\right) \frac{V_{cu} \sin\left(\xi_1 - \theta_1\right)}{\sin\left(\xi_1\right)} \tag{14}$$

the temperature rise at any point P(x, y, z) on the CHIP satisfies the following eq(15):

$$d\theta_t = \frac{B_1^c Q_{THS}}{2\pi\lambda} dl_i \left(\frac{1}{R_2} + \frac{1}{R_2^{'}} \right) dx_i \tag{15}$$

Where R_2 and R'_2 are the distances from the heat source and its image heat source to point P.

For a uniformly distributed strip heat source Q_{SHS} with a width of w and a length of l_0, the temperature rise at any point P (x, y, z) on the tool satisfies the following eq(16):

$$\theta_t = \frac{B_1^t Q_{THS}}{2\pi\lambda} \int_0^{l_0} dy_i \int_0^w \left(\frac{1}{R_2} + \frac{1}{R_2^{'}} \right) dz_i \tag{16}$$

3.2. Model of the Temperature Field on the Flank Face

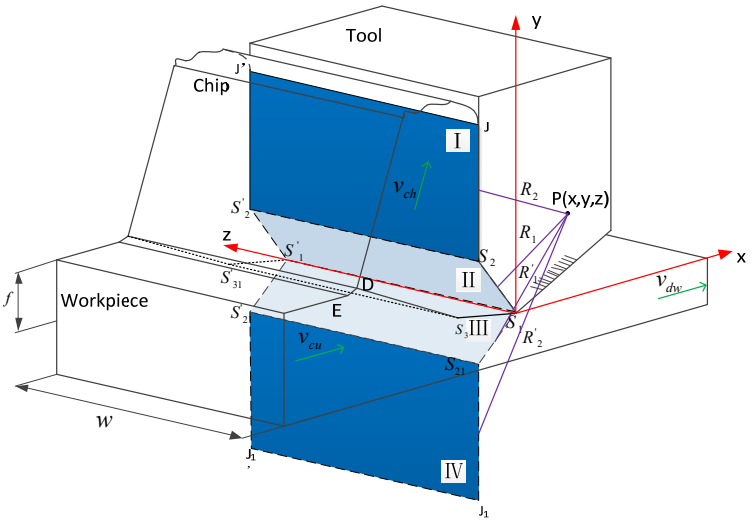

Figure 8. Heat Conduction Model of the Chamfered Tool

ISSN: 2710-0588

As shown in Figure 8, the temperature rise in the chamfered tool is mainly influenced by the Q_{SHS} and the Q_{THS} between DMZ and the chamfer boundary S_1S_2. To analyze the temperature rise, these two heat sources are considered as rectangular sources I and II with a width of w. Additionally, two symmetric image heat sources (III and IV) are introduced along the x-axis, and the temperature rise at any point on the rake face is determined by the combined effect of these four heat sources.

Based on Chao and Trigger's heat source model [19], a nonlinear heat distribution function B^t_i is introduced for analysis. The total temperature rise at any point P（x，y，z） on the tool is calculated using the following eq(17):

$$\theta_t = \begin{cases} \dfrac{B_1^t(1-S_m)Q_{THS}}{2\pi\lambda}\int_{l_i=0}^{l_0} dl_i \int_{lx_i=0}^{x_i=w}\left(\dfrac{1}{R_1}+\dfrac{1}{R'_1}\right)dx_i \\ +\dfrac{B_2^t Q_{SHS}}{2\pi\lambda}\int_{l_i=0}^{l_4} dl_i \int_{lx_i=0}^{x_i=w}\left(\dfrac{1}{R_2}+\dfrac{1}{R'_2}\right)dx_i \end{cases} \tag{17}$$

Here, 1-S_m represents the proportion of heat from the tool-workpiece friction heat source that flows into the tool. B^t_1 and B^t_2 are the non-uniform heat partition fractions for the friction heat sources at the DMZ-tool interface Q_{THS} and the chip-tool interface Q_{SHS}, respectively [7].

Due to the difference in material flow velocity between the two heat sources, different heat partition fractions need to be defined. B_{t1} and B_{t2} represent the heat partition fractions at the chip-tool interface on the rake face and the DMZ-tool interface, respectively. C_1 and C_2 are adjustment increments, while ΔB_1 and ΔB_2 are constant exponents related to the cutting conditions. Its definition is as follows [13] :

$$B_1^t = (B_{t1}+\Delta B_1) - 2\Delta B_1\left(\frac{l_1-l_i}{l_1}\right)^{m_1} - C_1\Delta B_1\left(\frac{l_1-l_i}{l_1}\right)^{k_1} \tag{18}$$

$$B_2^t = (B_{t2}+\Delta B_2) - 2\Delta B_2\left(\frac{l_{sl}-l_i}{l_{sl}}\right)^{m_2} - C_2\Delta B_1\left(\frac{l_{sl}-l_i}{l_{sl}}\right)^{k_2} \tag{19}$$

Due to different contact conditions between the chip-tool and DMZ-chamfer interfaces, their heat partition fractions differ. Which change with the temperature rise on the rake face. To better match the actual temperature variation, a power function term $c(l_i/l_1)^{ki}$ is added, where the value of m is adjusted between 0.22-0.26 to better reflect temperature changes when machining steel, particularly for l_i/l_1<0.4[14].

4. Finite Element Simulation Analysis

In this section, a simulation model for the chamfered tool machining of AISI-1045 workpiece is established. The simulation is conducted using DEFORM-2D, with the processing conditions constrained as shown in Fig9. The workpiece material is set with a length of 60mm and a height of 5mm. The tool in the model is treated as a rigid body, with the mesh distribution becoming finer closer to the tool tip. Two tools, a and b, with different geometric parameters, are set for simulation.

ISSN: 2710-0588

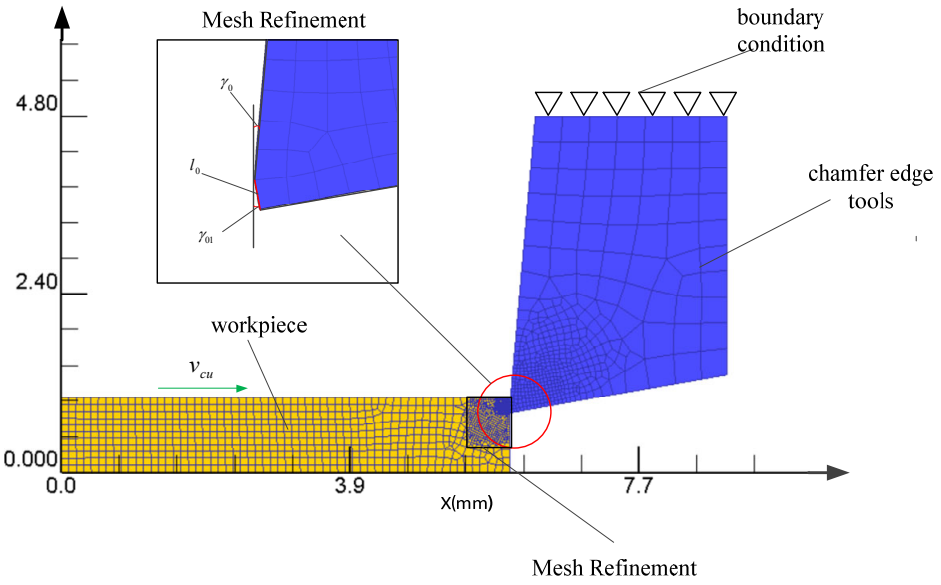

Figure 9. Finite Element Tool and Workpiece Constraint Setup

The cutting conditions are set as follows:

Table 2. Simulation Processing Parameter Setup

Test number	Rake-angle γ_0 (°)	Chamfer-angle γ_{01} (°)	Chamfer- length l_0 (mm)	cutter material
a	5	10	0.05	WC
b	3	35	0.2	

The cutting conditions are set as follows: tools *a* and *b* are configured with cutting speeds of 120 mm/sec and 170 mm/sec, respectively. The thermal conductivity of AISI-1045 is set to 50 W/m/K. The remaining processing parameters are listed in table 2.

4.1. Temperature Distribution of the Tool and Workpiece During the Cutting Process

When the cutting speed v=120m/min and the feed rate f=0.2mm/rev, the temperature distribution of the tool and workpiece during the machining process with Test *a* is shown in Fig.10.

Based on Fig.10, the temperature distributions in b and c show that the highest temperature on the tool occurs at the contact between the rake face and the chip, while the highest temperature on the chip is at the contact point with the rake face. This indicates that the tool-chip frictional heat source Q_{THS} has a significant effect on the temperature rise.

In Fig10(a), it can be observed that there is essentially no frictional heat generation within the DMZ. The temperature in this area is influenced by the flow of material temperature, which results in the temperature contour lines in the DMZ being relatively dense with a large gradient.

In Fig10.(b), it can be seen that friction between t boundary of DMZ and the workpiece generates frictional heat, leading to a significant temperature difference. This confirms the existence of the Q_{THS} impact on temperature. Furthermore, it is also clear that the temperature rise effects in the workpiece, occurring in the main shear zone and below the DMZ, show distinct differences under various cutting speeds: in low-speed cutting, the temperature gradient in the workpiece is more widely distributed compared to high-speed cutting, where the workpiece exhibits a higher temperature gradient and more concentrated temperature changes.

ISSN: 2710-0588

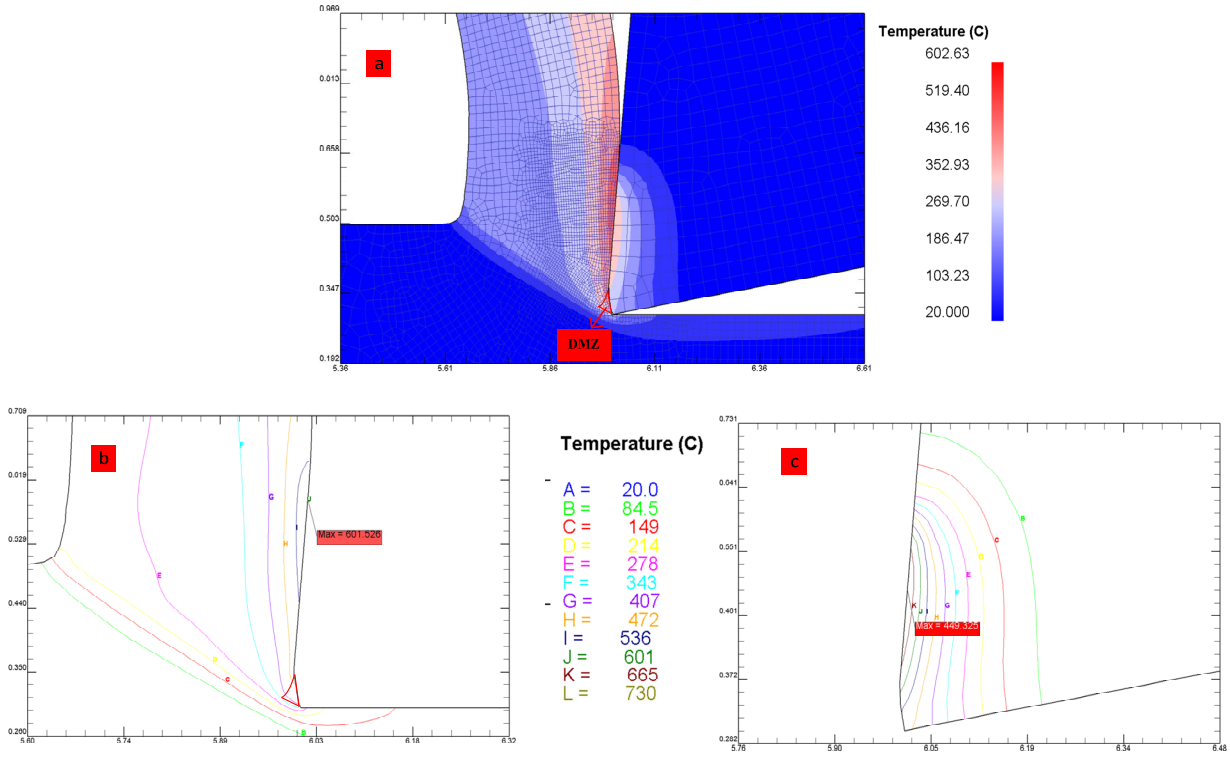

Figure 10. Temperature Distribution During Tool Machining in FE Simulation: (a) Overall Cutting Temperature Distribution in Finite Element Simulation. (b) Chip Temperature Distribution in FE Simulation (c) Tool Temperature Distribution in FE Simulation

4.2. Analysis of Flank Face Temperature Calculation

Based on eqs (5), (9), and (14), the thermal analysis model was solved using MATLAB to calculate the tool rise of temperature. The obtained stress and thermal intensity results are shown in Table 3.

Table 3. The thermal intensity of the tool.

Test number	cutting speed mm/sec	Q_{THS} (J/mm²s)	Q_{PHS} (J/mm²s)
a	120	56903	142342
	170	70783	177063
b	120	66458	119963
	170	84345	152253

The temperature distribution on the flank face of tools a and b at different cutting speeds is shown in Figure 11.

ISSN: 2710-0588

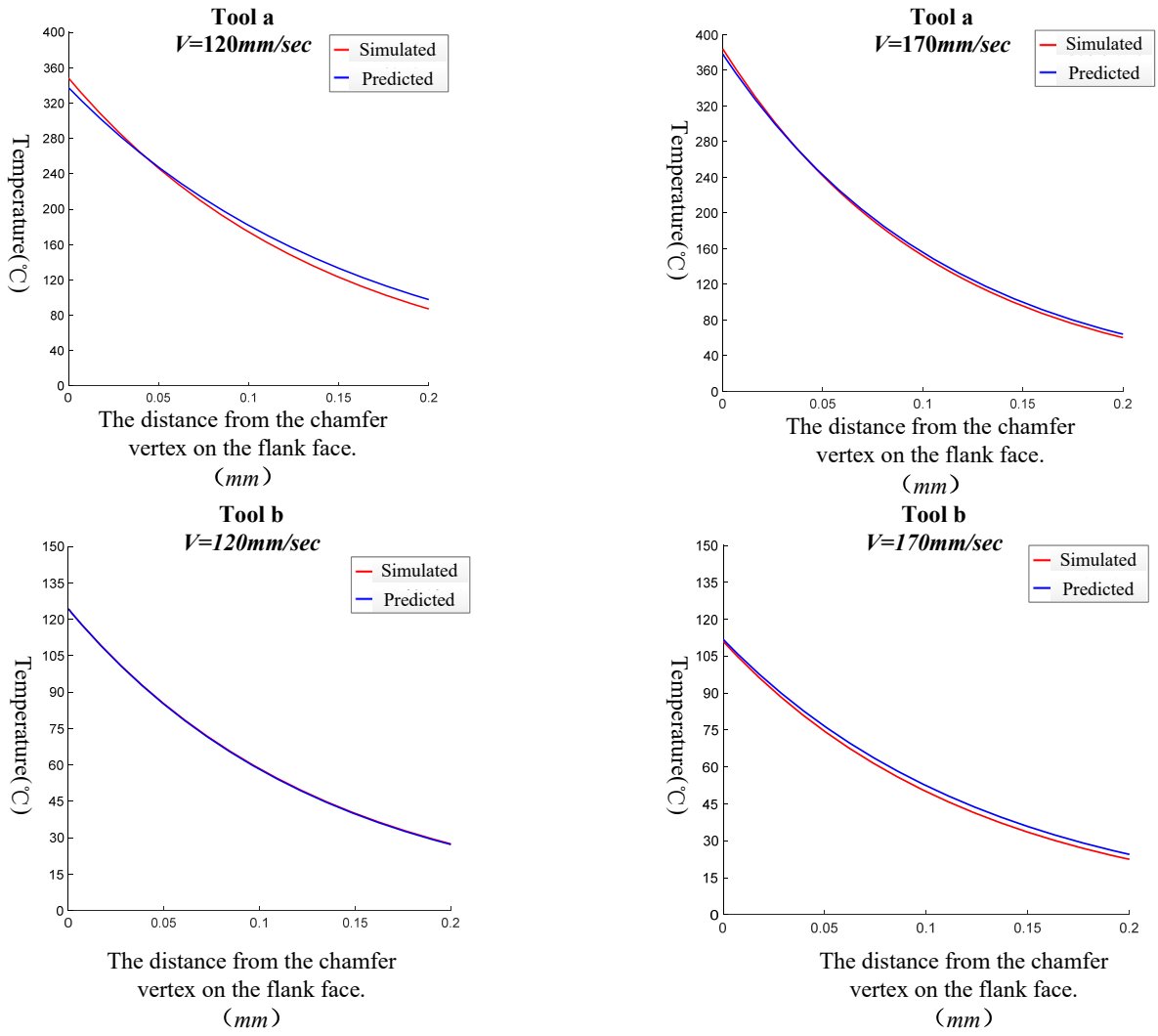

Figure 11. Temperature distribution variation diagram of the flank face.

The theoretical calculations of flank face temperature magnitude and variation trend align with the simulation results. The temperature distribution trend shows a gradual decrease from the chamfer apex S_1 towards the rear of the tool, with the highest temperature occurring at the intersection of the chamfer and rake face S_1. This indicates that the Q_{THS} generated DMZ and the Q_{SHS} have a significant influence on temperature rise.

Under different cutting speed conditions, higher temperatures can cause material softening at the DMZ boundary, altering the friction coefficient between materials. As the friction coefficient decreases, lower temperatures may be observed under certain cutting conditions. It is important to is discrepancies exist between this temperature distribution and the actual temperature distribution. This is because the temperature field in DEFORM-2D is time-dependent and considers heat conduction the tool-chip. When using the same temperature interval, noticeable deviations can be observed. However, these deviations are present only within the tool and not at the tool-chip contact interface.

The variation of the heat partition fractions B_{t1} and B_{t2} with respect to the distance from the tool tip edge is shown in Fig.11.

ISSN: 2710-0588

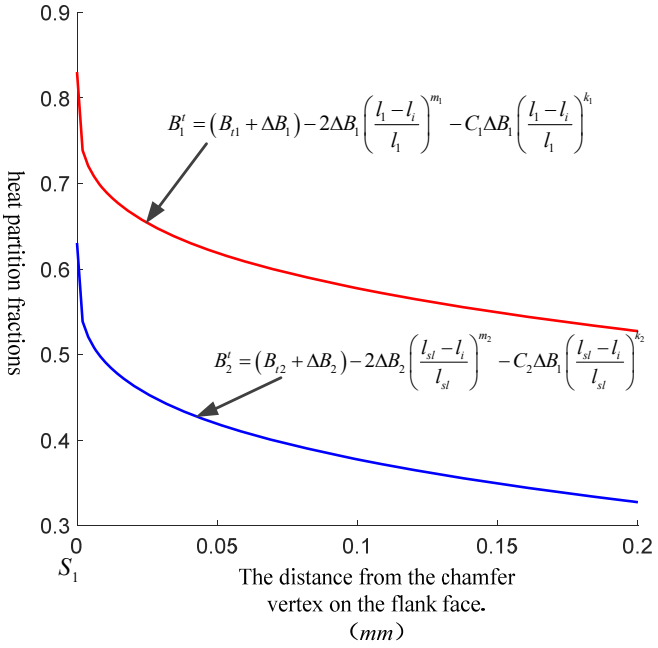

Figure 11. The variation of heat partition fractions on the flank face

These heat partition fractions are manually adjusted during the calculation of the flank face temperature to match the results of the temperature field analysis, corresponding to the heat sources \(Q_{THS} and Q_{SHS}. AISI-1045, as a medium-carbon steel, has a high Peclet number, range of N_{pe}=5-20 [15]. When ΔB= 0.3, the values of B_{t1} and $B_{t2}$are nearly equal, indicating that the effects of the tool-chip and tool-DMZ interactions are approximately the same at this point.

5. Results

This paper, based on the orthogonal cutting model of chamfered tools, establishes the relationship between cutting force and cutting speed due to the effect of DMZ. Furthermore, it determines the size of the cutting heat sources based on this relationship. Using the heat source method, the temperature on the tool is calculated, resulting in the temperature field distribution on the rake face. Additionally, the temperature and variation trends on the flank face, as well as the values of the heat partition fractions, are computed. Finally, the validity of the theoretical model is verified through finite element simulations.

References

[1] Merchant M E. Mechanics of the metal cutting process. I. Orthogonal cutting and a type 2 chip[J]. Journal of applied physics, 1945, 16(5): 267-275.

[2] Oxley P L B, Welsh M J M. An explanation of the apparent Bridgman effect in Merchant's orthogonal cutting results[J]. 1967.

[3] Fang N. Machining with tool–chip contact on the tool secondary rake face—Part I: a new slip-line model[J]. International journal of mechanical sciences, 2002, 44(11): 2337-2354.

[4] Fang N. Machining with tool–chip contact on the tool secondary rake face—Part II: analysis and discussion[J]. International journal of mechanical sciences, 2002, 44(11): 2355-2368.

[5] Karpat Y, Özel T. An integrated analytical thermal model for orthogonal cutting with chamfered tools[J]. Trans. NAMRI/SME, 2006, 34: 9-16.

ISSN: 2710-0588

[6] Hu C, Zhuang K, Weng J, et al. Cutting temperature prediction in negative-rake-angle machining with chamfered insert based on a modified slip-line field model[J]. International Journal of Mechanical Sciences, 2020, 167: 105273.

[7] Zhuang K, Zou L, Weng J, et al. Occurrence of catastrophic tool wear patterns through systematic thermomechanical modeling[J]. Journal of Manufacturing Processes, 2024, 109: 288-299.

[8] Hitomi K. Fundamental machinability research in Japan[J]. 1961.

[9] Jacobson S, Wallén P. A new classification system for dead zones in metal cutting[J]. International Journal of Machine Tools and Manufacture, 1988, 28(4): 529-538.

[10] Wan M, Wen D Y, Ma Y C, et al. On material separation and cutting force prediction in micro milling through involving the effect of dead metal zone[J]. International Journal of Machine Tools and Manufacture, 2019, 146: 103452.

[11] Wu S, Wang D, Zhang J, et al. Study on the formation mechanism of cutting dead metal zone for turning AISI4340 with different chamfering tools[J]. Micromachines, 2022, 13(7): 1156.

[12] Komanduri R, Hou Z B. Thermal modeling of the metal cutting process: part I—temperature rise distribution due to shear plane heat source[J]. International Journal of Mechanical Sciences, 2000, 42(9): 1715-1752.

[13] Komanduri R, Hou Z B. Thermal modeling of the metal cutting process—Part II: temperature rise distribution due to frictional heat source at the tool–chip interface[J]. International Journal of Mechanical Sciences, 2001, 43(1): 57-88.

[14] Komanduri R, Hou Z B. Thermal modeling of the metal cutting process—Part III: temperature rise distribution due to the combined effects of shear plane heat source and the tool–chip interface frictional heat source[J]. International Journal of Mechanical Sciences, 2001, 43(1): 89-107.

[15] Karpat Y, Özel T. Analytical and thermal modeling of high-speed machining with chamfered tools[J]. 2008.

[16] Yin G, Shen J, Wu Z, et al. Experimental investigation on the machinability of PCBN chamfered tool in dry turning of gray cast iron[J]. Processes, 2022, 10(8): 1547.

[17] Hussain G, Alkahtani M, Alsultan M, et al. Chip formation, cutting temperature and forces measurements in hard turning of Gcr15 under the influence of PcBN chamfering parameters[J]. Measurement, 2022, 204: 112130.

[18] Dewhurst P. A general matrix operator for linear boundary value problems in slip-line field theory[J]. International journal for numerical methods in engineering, 1985, 21(1): 169-182.

[19] Jaeger J C. Moving sources of heat and the temperature at sliding contacts[J]. Proc. Roy. Soc. New South Wales, 1942, 76: 203.